REVIEW   **Open Access**

Inertial sensors technologies for navigation applications: state of the art and future trends

Naser El-Sheimy [ID] and Ahmed Youssef*[ID]

Abstract

Inertial navigation represents a unique method of navigation, in which there is no dependency on external sources of information. As opposed to other position fixing navigation techniques, inertial navigation performs the navigation in a relative sense with respect to the initial navigation state of the moving platform. Hence, inertial navigation systems are not prone to jamming, or spoofing. Inertial navigation systems have developed vastly, from their occurrence in the 1940s up to date. The accuracy of the inertial sensors has improved over time, making inertial sensors sufficient in terms of size, weight, cost, and accuracy for navigation and guidance applications. Within the past few years, inertial sensors have developed from being purely mechanical into incorporating various technologies and taking advantage of numerous physical phenomena, from which the dynamic forces exerted on a moving body could be computed accurately. Besides, the evolution of inertial navigation scheme involved the evolution from stable-platform inertial navigation system, which were mechanically complicated, to computationally demanding strap-down inertial navigation systems. Optical sensory technologies have provided highly accurate inertial sensors, at smaller sizes. Besides, the vibratory inertial navigation technologies enabled the production of Micro-electro-machined inertial sensors that are extremely low-cost, and offer extremely low size, weight and power consumption, making them suitable for a wide range of day-to-day navigation applications. Recently, advanced inertial sensor technologies have been introduced to the industry such as nuclear magnetic resonance technology, cold-atom technology, and the re-introduction of fluid-based inertial sensors. On another note, inertial sensor errors constitute a huge research aspect in which it is intended for inertial sensors to reach level in which they could operate for substantially long operation times in the absence of updates from aiding sensors, which would be a huge leap. Inertial sensors error modeling techniques have been developing rapidly trying to ensure higher levels of navigation accuracy using lower-cost inertial sensors. In this review, the inertial sensor technologies are covered extensively, along the future trends in the inertial sensors' technologies. Besides, this review covers a brief overview on the inertial error modeling techniques used to enhance the performance of low-cost sensors.

Keywords: Gyroscopes, Accelerometers, Optical inertial sensors, Micro-electro-machined, Fluid-based inertial sensors, Stochastic modeling

Introduction

The state of motion of any moving platform could be determined through a process known as Navigation. Whereas, navigation is done by determining the navigation states of the moving platform. The navigation states represent the position, velocity, and orientation of the platform in either two-dimensional (2-D) or three-dimensional (3-D) space [1].

Navigation techniques are classified into two major categories. Namely, position fixing and dead reckoning. Position fixing is performed by determining the navigation states with respect to a set of well-known positions. An example of position fixing technique is the global navigation satellite systems (GNSS). On the other hand, dead reckoning determines the navigation states of a moving platform by measuring recursively the progression of

*Correspondence: ahmed.youssef1@ucalgary.ca
Mobile Multi-sensor Systems Research Team, Department of Geomatics Engineering, University of Calgary, 2500 University Drive N.W, Calgary, AB T2N 1N4, Canada

such navigation states with respect to their initial values. Inertial navigation is an example of the dead reckoning navigation technique [1].

The need for dead-reckoning navigation arises from the limitations of typical position fixing techniques which require a direct line of sight between the platform, to be navigated, and the well-known fixed positions. To clarify, navigation using GNSS requires a direct line of sight between the GNSS receiver and at least four satellites to acquire the navigation states of the navigated platform. Such condition is not usually met practically, especially when navigation takes place in urban or indoor environments. Consequently, GNSS-denied environments require the use of dead-reckoning, especially inertial navigation, to provide a navigation solution for periods in which position fixing solution is not possible [2].

If one could measure the resultant force exerted on a moving body, and deploy Newton's second law of motion, the linear and/or rotational rates of motion could be deduced. Hence, inertial sensors emerge. Inertial sensors are classified into two main categories: accelerometers and gyroscopes. Broadly, accelerometers measure specific forces or accelerations, while, gyroscopes measure angular velocities.

When fitted into specific geometric forms that guarantees capturing the motion of any given platform, the inertial sensors assembly is referred to as an inertial measurement unit (IMU). Whereas, IMUs are usually coupled with some form of basic on-board data processing to convert the raw measurements to sensible specific forces or angular velocities. A typical IMU comprises a triad of accelerometers and a triad of gyroscopes mounted along three mutually orthogonal axis to capture the 3-D motion of any given platform to which it is mounted.

Nevertheless, inertial navigation is done by processing the inertial measurements that are acquired from IMUs. The inertial measurements are mathematically reduced into variations in position, velocity, and orientation for the moving platform. Consequently, the navigation states could be accumulated over time to identify the position, velocity, and orientation of the platform at any given instant. Therefore, a system that utilizes the measurements of IMUs to acquire the navigation states of any moving platform to which it is mounted is known as an inertial navigation system (INS). An INS is a system that would include an IMU along with some means to process the inertial measurements into a full navigation solution.

Inertial sensors suffer from errors, which are either systematic errors or random errors. Systematic errors can be modeled mathematically and can be mitigated through calibration. Systematic errors, in inertial sensors, include biases scale factor, scale-factor non-linearity, and cross-coupling of sensitive axes measurements. A bias in an inertial sensor is a constant shift in the measured quantity from the actual input to the sensor. Whereas, a scale factor is an error that represents the mismatch between the input quantity to an inertial sensor, and the reported output quantity of the sensor. Typically, one should expect an inertial sensor to report an output value equivalent to whichever input value imposed upon the sensor. Hence, the expected input–output ratio should be equal to one. However, a scale factor would manifest as deviation of the input–output relation of an inertial sensor from being equal to one. Another form of the systematic errors is the scale-factor non-linearity. Typically, the input–output relation of a sensor is expected be a linear relation. However, due to environmental impacts and some sensors designs, the input–output relation ship of the inertial sensor might not be a linear relation, which is a systematic error that should be accounted for. Due to improper mounting of inertial sensors within a geometric assembly of an IMU, cross-coupling error occurs. Cross-coupling is caused by the non-orthogonality of the sensitive axes of inertial sensors. Consequently, the inertia sensors (either accelerometers or gyroscopes) measure residual inertial measurements from another axis that is supposed to be orthogonal to its sensitive axis [3].

Evidently, inertial sensors endure random errors that would manifest as noises within the inertial measurement signals acquired from inertial sensors. The random errors can be attributed to electrical or mechanical sources, depending on the design and manufacturing of the inertial sensors. Nonetheless, the order of magnitude and impact of such random errors on the inertial navigation solution is dependent upon the technology, design, and manufacturing techniques of the inertial sensors. Consequently, the performance of any given IMU in terms of providing an accurate navigation solution is defined by the order of magnitude of the systematic and random errors included in its measurements. Hence, IMUs are classified into grades as per their performance and accuracy.

However, it is understandable that there exists a high correlation between the performance of any given IMU, its underlying technology, and its cost. Whereas, IMUs are classified into: strategic, navigation, tactical, and consumer grades. Table 1 provides a summary of IMUs classification as per performance, accuracy, and cost, which is modified after [1]. It is noted that performance parameters upon which the IMUs are classified are discussed afterwards.

Table 1 A summary of IMUs classification as per performance, from [1]

Grade	Strategic grade	Navigation grade	Tactical grade	Commercial grade[a]
Positional error	30–100 m/h	1 nmi[b]/h or 0.5 m/s	10–20 nmi/h	Large variation
Gyroscope drift	0.0001–0.001°/h	<0.01°/h	1–10°/h	0.1°/s
Gyroscope random walk	–	$< 0.002°/\sqrt{h}$	$0.05-<0.02°/\sqrt{h}$	Several $°/\sqrt{h}$
Accelerometer bias	0.1–1 µg	<100 µg	1–5 mg	100–1000 µg
Applications	Submarines Intercontinental ballistic missiles	General navigation High precision georeferencing Mapping	Integrated with GPS for mapping Weapons (Short time)	Research Low cost navigation Pedometers Anti-locking breaking Active Suspension Airbags
Cost	~$1 million	~$100,000	~$2000–$50,000	$1 for accelerometers $10 for gyroscopes

[a] Also called automotive grade

[b] 1 nautical mile (nmi) ≈ 6076 ft ≈ 1851 m

This paper introduces an overview over the classification of the INSs based on their operation mode, into either stable-platform or strap-down INSs, as shown in "General classification of inertial navigation systems" section. The differentiation between the two categories of INSs resides in the mechanical system mounts, and mathematical process implemented to acquire a full navigation solution and their differences. "Inertial navigation technologies" section covers an overview on the state-of-the-art inertial sensor technologies, and a historical overview over the development of inertial sensor technologies. "Future trends in inertial sensors technologies" section provides a summary of future trends in inertial navigation sensor technologies. "Stochastic error modeling for inertial navigation" section covers an overview on the stochastic error modeling methods, with which inertial sensor errors are modeled into navigation algorithms, which is a major aspect of acquiring an error-bounded navigation solution from a dead-reckoning INS.

General classification of inertial navigation systems

Another form of classifying the INSs is depending on their mechanical operation scheme. INSs can be classified into stable platform INSs, and strap-down INSs. An argument can be made that this classification is a chronological one. Whereas, the stable platform INSs have been gradually replaced over the years by the strap-down INSs. However, stable platform INSs are not being entirely replaced, and are still used for some navigation applications. Stable platform INSs are commonly referred to as mechanical INS, as discussed hereafter. Figure 1 shows a schematic of the difference between stable-platform and a strapdown INSs, from [1].

Stable-platform inertial navigation systems

This type of INSs require mounting the inertial sensors on a stable platform that is mechanically isolated from the rotational motion of the vehicle. Such requirement
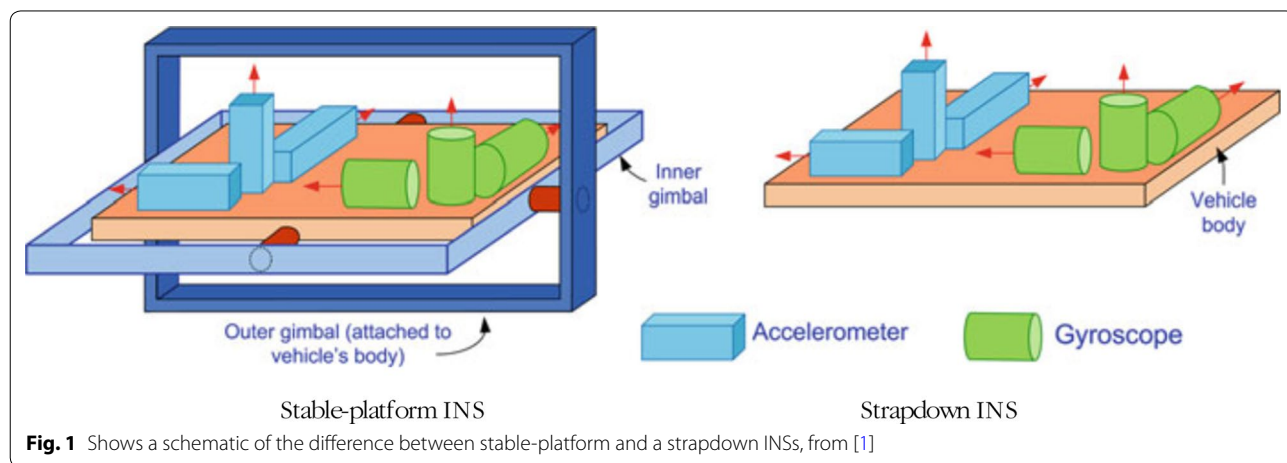

Fig. 1 Shows a schematic of the difference between stable-platform and a strapdown INSs, from [1]

could be achieved by utilizing mechanical inertial sensors, specifically gyroscopes. Within its internal structure and mechanism, a typical mechanical gyroscope comprises a rotating rotor means, with high moment of inertia about a given spin axis, which is rotated by mechanical means, and are presumed to maintain high rotational speeds. These conditions lead such rotor to maintain spatial rigidity in space, as per the law of conservation of momentum. Such spatial rigidity of the rotor allows it to maintain a stable direction in space. A gimbal connection is connected to said rotor means, which typically constitute three free rings connected through pure hinged connections and are free to rotate in 3D. Consequently, the rotation rate of the moving platform can be detected by utilizing a pick-off means to determine the rotation of the gimbal tings with respect to the spatially rigid rotor [4].

Nonetheless, mechanical gyroscopes were the means to provide a mechanically stable platform that helped realize inertial navigation in the first place. It is noted that such theoretical assumption of having a stable spin axis direction for the mechanical gyroscope rotor was not entirely satisfied practically. Whereas, mechanical INSs suffered from various sources of errors. Chief among those errors, is the precession error caused by externally applied torques to the spinning rotor which would in turn affect its spatial rigidity in space and would lead the rotor to deviate from its assumed direction [4]. Such external torques could be caused by improper balance of masses within the gyroscope design, or under the impact of external shocks. Despite that, stable platform INSs are considered very accurate and reliable. Whereas, stable platform INSs are still used for applications that require very accurate estimates of navigation data such as ships and submarines. However, the downsides of such systems are being large in size, being of high cost, and having high mechanical complexity.

Strap-down inertial navigation systems

A modern alternative for the stable-platform INSs are the strap-down INSs. From the nomenclature, strapdown INSs imply that the inertial sensors are strapped down rigidly to the vehicle to which they are mounted. Generally, it is noted that the concept of inertial navigation depends of acquiring inertial measurements of the moving vehicle with respect to an inertial non-rotating non accelerating reference coordinate system, or frame. However, the navigation states should be represented with respect to a navigation frame. Hence, for stableplatform INSs, such measurements are acquired by utilizing the mechanical stabilization of the inertial sensors as explained in the previous "Stable-platform inertial navigation systems" section. However, for strap-down INSs, the mechanical stabilization that was provided within stable-platform systems are replaced by a computational model to achieve the same output navigation states. Since, the computational model of strap-down INSs is a mathematical realization of the mechanical stabilization in mechanical systems, it is referred to as INS mechanization [4].

INS Mechanization can be defined as the process by which Newton's law of motion are applied, along with the geometric transformations of reference frames, to acquire the required navigation states from IMU measurements. The navigation states include the position, velocity, and attitude of the moving platform.

INS Mechanization in general can be realized using any set of sensors that would be able to provide the raw measurements, that when processed can give the navigation states within the chosen reference frame dimensions (i.e. 1-D dimensional, 2-D, or 3-D navigation frames).

Consequently, the mechanization process transforms the measurements to the navigation frame as a basic component of the process. Then, the mechanization process includes an integration over time to acquire the navigation states from the raw measurements of the IMU. Such measurements include the rotation rates from the gyroscopes that are integrated to acquire the attitude angles, and the specific forces from the accelerometers that are integrated to acquire the velocities and the positions [1].

Strap-down INSs comprise most of the state-of-the-art INSs. Strap-down INSs provide optimal alternative for the stable-platform INSs, because strap-down systems provide lower cost, smaller size INSs, that have comparable reliability to the stable-platform systems. Besides, strap-down INSs remove most of the mechanical complexity associated with the stable-platform systems. Such advantages enable the strap-down INSs to be utilized for a wider range of applications, that demand high performance and light weight. On the other hand, strap-down systems endure some drawbacks that include the substantial increase in computational complexity and high demand for on-board processing power. However, due to recent advances in computer technology with the development of suitable sensors, such strap-down systems have been successfully realized, and dominate the major aspects in the state-of -the-art inertial navigation.

Inertial navigation technologies

There are numerous technologies that comprise the state-of-the-art commercialized inertial sensors that are utilized to build strapdown INSs. However, there are basic technologies which dominate the market of inertial

navigation. In this section, the dominant state-of-the-art technologies in inertial navigation are discussed in terms of sensor basic operation principles and expected performances. This section highlights the main technologies for angular rate sensors, and accelerometers, as well.

An inertial sensor, regardless of its underlying technology, comprises three main components that constitute a fully-functional inertial sensor. An inertial sensor includes a motion transduction mechanism, a signal conditional mechanism, and a sensor read-out component [5].

A motion transduction mechanism is responsible for detecting the physical phenomenon upon which the inertial sensor operates and transforms such detection into a quantifiable signal. Hence, a motion transduction mechanism includes a motion indicator, or a sensing element, a pick-off mechanism, and a damping mechanism [5]. The motion indicator of an inertial sensor represents the seismic element that reacts to any externally applied motion. A pick-off mechanism represents the means by which the reaction of the motion indicator is detected and transformed into a signal. Whereas, a damping mechanism is responsible for restoring the sensing element to its null position whenever the external stimulus is unapplied to the sensor. It is noted that the damping mechanism depends mainly on the design configuration of the inertial sensor.

To clarify, an inertial sensor could be design with either an open-loop or closed-loop design configuration. Whereas, an open-loop design configuration relies on the physical phenomenon upon which the sensor operates to restore its sensing element to its null state without any interference from an external source, depending solely on the governing physical equilibrium. On the other hand, a closed-loop design configuration provides an external source of balance that provides a feedback to the sensor's sensing element to restore it to its null state, and is referred to in literature as the feedback, or rebalance, loop. Closed-loop inertial sensors generally provide higher sensitivity sensors with low order of magnitude errors; however, it can be characterized of being relatively high cost in comparison to open-loop inertial sensors.

Nevertheless, a signal conditioning mechanism is a means by which the detected signal from the pick-off mechanism is converted into the desired measurable quantity from an inertial sensor (i.e., specific forces for accelerometers, or angular rates for gyroscopes). Whereas, a sensor read-out is the interface by which the measured quantities are conveyed to the user. However, a sensor read-out is not often considered as a core component of an inertial sensor, as it varies as per the intended application for the inertial sensor.

Angular rate sensors technologies

As stated earlier, an IMU comprises an angular rate sensor that is used to measure the angular rates of any moving platform, form which the attitude of the platform is determined. Angular rate sensors vary over a large range of accuracy, which can be described holistically by bias of the angular rate sensors. The range of biases encountered with different angular rate sensors vary from less than 0.0001°/h up to 1°/s class or worse. Generally, most angular rate sensors are sensitive to their operation environment, which leads to some undesirable effects.

Dynamically tuned gyroscopes (DTG)

State-of-the-art angular rate sensors vary in terms of the utilized technologies and operation principles, which in turn is representative of their accuracy. Angular rate sensors include mechanical-based gyroscopes, which are modernized to be used in strapdown mode, such as dynamically tuned gyroscopes (DTG), and flex gyroscopes [4]. Such type of gyroscopes basically operates using a highly spinning mass. However, in these strapdown-type sensors, the operation concept relies on the gyroscopic precession effect that occur because of external torques acting upon a spinning mass. The torques are applied intentionally to the spinning mass, using restraining means as hinges or the like. Consequently, the spinning mass precession is considered as a measure of the angular rate, which is measured using appropriate pick-off means. Figure 2 shows a schematic 3D view of a DTG, modified after [4].

Vibratory gyroscopes

Another technology for angular rate sensors fabrication is the vibratory gyroscopes. The operation principle of vibratory gyroscopes was discovered by Foucault [4]. The operation principle of the vibratory gyroscopes implies that a vibrating element, such as a rod, maintains its plane of vibration regardless of the motion of the sensor
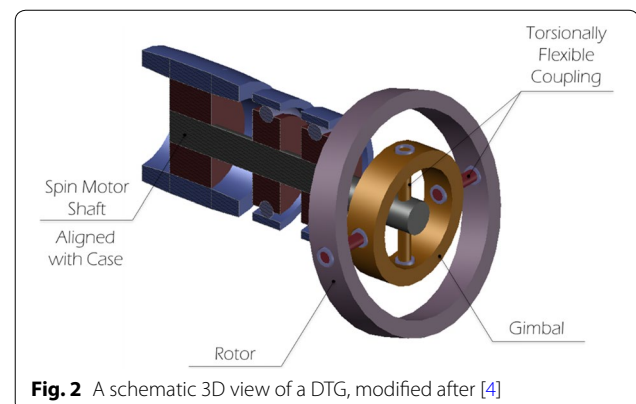
Fig. 2 A schematic 3D view of a DTG, modified after [4]

in space. Consequently, the angular rates and linear accelerations can be measured relying on such concept. The vibrating element can take various forms, such as: a string, hollow cylinder, rod, tuning fork, beam, and hemispherical dome. To clarify, the vibratory motion of an element creates an oscillatory linear velocity. If the sensor is rotated about an axis orthogonal to the oscillatory linear velocity, a Coriolis acceleration is induced, which modifies the motion of the vibrating element. If such motion variations, due to Coriolis force, can be detected and measured, the angular rate can then be deduced. The vibratory gyroscopes can be characterized by its susceptibility to be miniaturized and being mass produced at relatively cost. Hence, vibratory gyroscopes can be considered as the base technology upon which micro-electro-mechanical-system (MEMS) based gyroscopes are produced. However, vibratory gyroscopes can be characterized by having high drift rates, limits on input range of the gyroscopes due to limits of natural frequency of the resonator (i.e., vibrating element), and sensitivity to environmental effects such as temperature variations and

shocks. Figure 3 shows a schematic 3D view of a vibratory fork gyroscope, as an example of vibratory gyroscopes, modified after [4].

Optical gyroscopes

One of the most effective and accurate technologies in gyroscopes fabrication is the optical gyroscopes. The operation concept of the optical gyroscopes depends on the Sagnac Effect. The Sagnac effect implies that, for a closed loop interferometer, the phase of light traveling within the interferometer is proportional to the external angular rate, to which it is subjected. Optical gyroscopes can be realized in many forms, most effective of which are ring laser gyroscopes (RLG), which represents an active optical gyroscope architecture, and fiber optics gyroscopes (FOG), which represents a passive optical gyroscope architecture [6].

To clarify, the FOG gyroscope consists of a Fiber Optics cable coiled in a closed form. For simplicity, the Fiber Optics cable is coiled into one turn; however, typically it is turned into more than one turn. It is noted that the number of turns affects the sensitivity of the Gyroscope. Nevertheless, the FOG gyroscope also consists of a light source, light detector, and a set of coupling lenses. The light source emits light which passes through a beam splitter. The light waves, afterwards, flow into two opposing paths, and are then rejoined through the beam splitter towards the light detector. The interference pattern of the two sets of light beams remains constant, as per the detector, until the gyroscope is subjected to an external rotation about its sensitive axis [6]. Afterwards, the interference pattern varies with a magnitude proportional to the angular rate. Table 2 provides a summary of typical performance characteristics for a range of angular rate sensors suitable for strapdown application, from [4]. Whereas, Fig. 4 shows a very simple schematic of a single turn FOG, to clarify the operation concepts and main components of FOG.
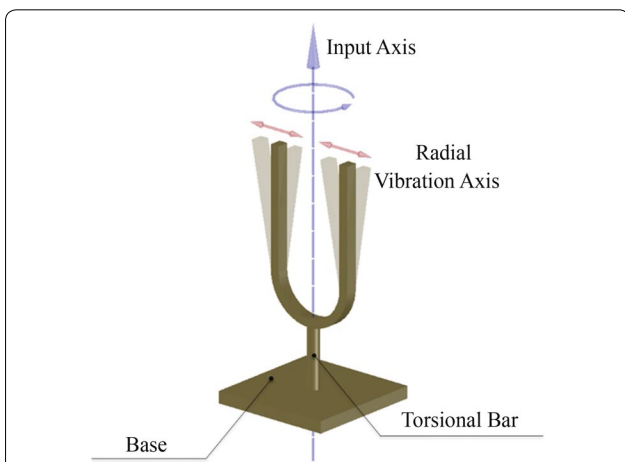
Fig. 3 A schematic 3D view of a vibratory fork gyroscope, as an example of vibratory gyroscope, modified after [4]

Table 2 A summary of typical performance characteristics for a range of angular rate sensors suitable for strapdown application, from [4]

Characteristic	DTG	Flex gyro	Vibratory gyro	RLG	FOG
g-Independent bias (°/h)	0.05–10	1–50	360–1800	0.001–10	0.5–50[a]
g-Dependent bias (°/h/g)	0.01–10	1–10	36–180	0	< 1
An-isoelastic bias (°/h/g^2)	0.1–0.5	0.05–0.25	18	0	< 0.1
Scale-factor non-linearity (%)	0.01–0.1	0.01–0.1	0.2–0.3	5–100	0.05–0.5
Bandwidth (Hz)	100	200	500	> 200	> 100
Maximum input rate (°/s)	1000	> 500	> 1000	> 1000	> 1000
Shock resistance	Moderate	Moderate	> 25,000 g	Good	Good

[a] For high-end interferometric FOG, the bias instability < 0.0003°/h, random walk < 0.00008 $°/\sqrt{h}$, and scale factor of < 0.5 ppm

Fig. 4 A very simple schematic of the main components of a FOG
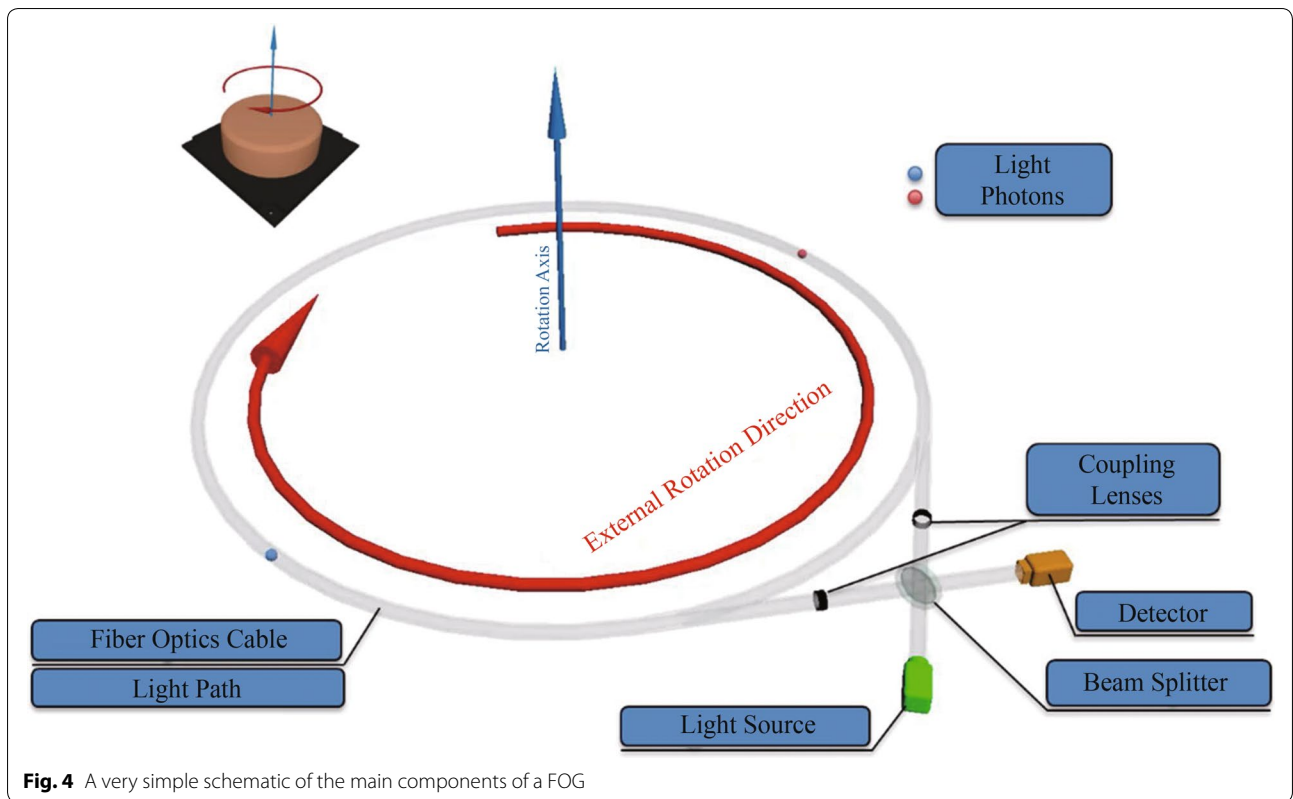
It is noted that gyroscopes performance and costs are directly related to the applications requirements, and the utilized technologies therewith. Figure 5 shows the relation between the scale factor instability in parts per million (ppm) which reflects the quality of the gyroscopes in depicting angular rates without being sensitive to undesirable impacts, as a function of the bias stability expressed in (°/h), which is intrinsically a quantity

representative of the gyroscope technology and the associated noises therewith [6].

Fluid-based angular rate sensors

Whereas, for fluid-based angular rate sensors, the sub-categorization includes: rate integrating gyroscopes (RIGs), dual-axis rate transducers (DART), magnetohydrodynamic (MHD) angular rate sensors, jet flow angular
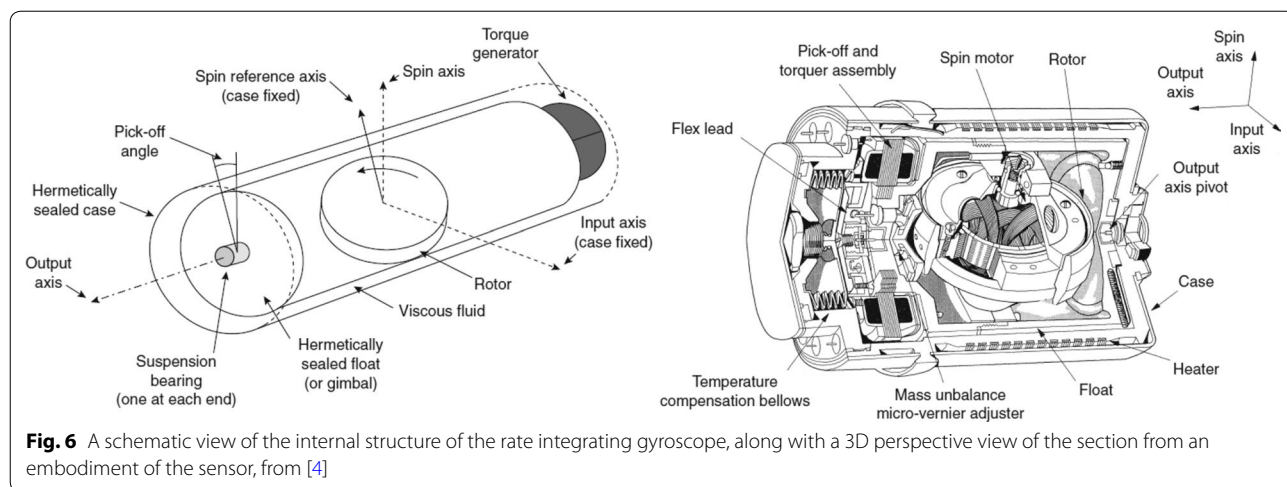

Fig. 5 The relation between the scale factor instability in parts per million (ppm) as a function of the bias stability expressed in (°/h), from [6]
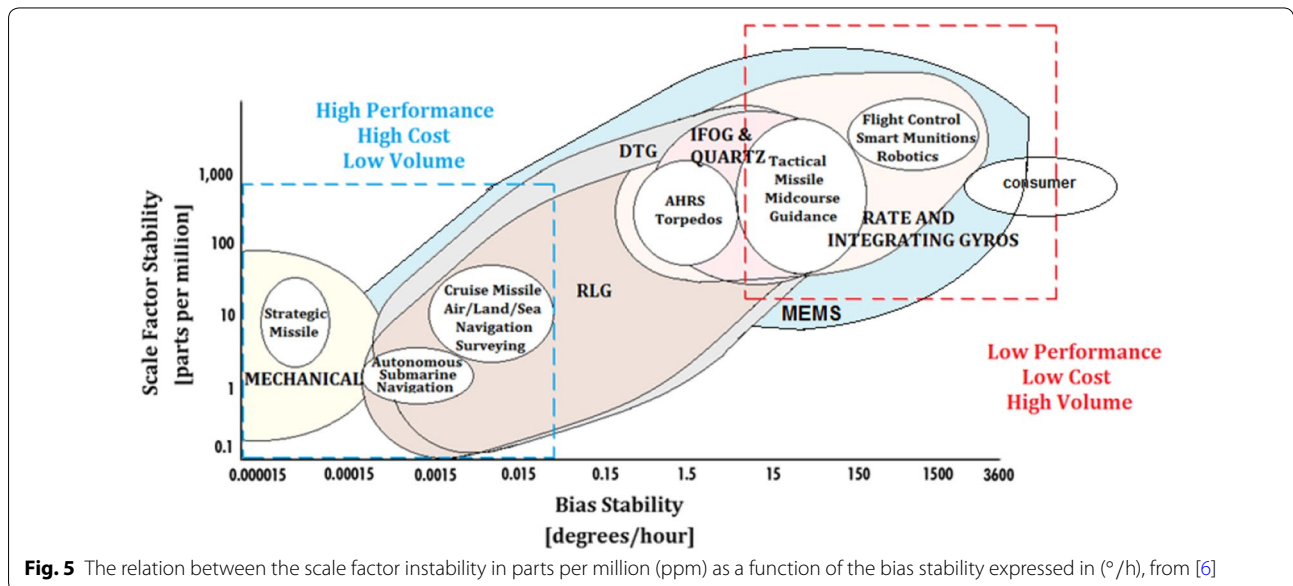
Fig. 6 A schematic view of the internal structure of the rate integrating gyroscope, along with a 3D perspective view of the section from an embodiment of the sensor, from [4]

rate sensors, porous fluid flow gyroscopes, and vortex rate gyroscopes, integrating angular accelerometers, micromachined fluid-based gyroscopes (thermal gas gyroscopes), and micromachined biomimetic gyroscopic sensors.

Rate integrating gyroscopes   RIGs were initially introduced in the 1960s. Many US patents were introduced in such period, developing various versions of rate integrating gyroscopes, such as [7–12]. Nonetheless, RIGs do not implement fluid as its inertial mass. However, RIGs make use of the fluid properties, and the conservation of momentum to measure the angular velocity. RIGs use a high-rate spinning rotor with high moment of inertia to keep its spin axis fixed in 3-D, unless affected by external torque. In such case, the rotor would precess, and the spin axis would follow the direction of the applied torque axis [4]. Figure 6 shows a schematic view of the internal structure of the rate integrating gyroscope, along with a 3D perspective view of the section from an embodiment of the sensor, from [4].

Magnetohydrodynamic gyroscopes   MHD angular rate sensors make use of the magnetohydrodynamic effect in conductive fluids, such as mercury, to detect the angular rates. The magnetohydrodynamic effect is the induction of electric current into a fluid, because of being subjected to varying magnetic fields. The induced current can polarize the flow, which in turn affect the applied magnetic field itself. The magnetohydrodynamic effect can be mathematically modeled using the Navier–Stokes equations for momentum conservation for incompressible fluids, and Maxwell's equations for electromagnetism. The variations in the magnetic field are detected as indication of the external angular motion imparted to these types of sensors [4].
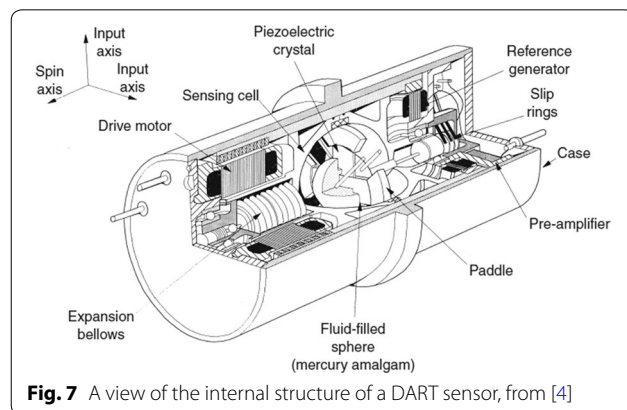

Fig. 7 A view of the internal structure of a DART sensor, from [4]

Dual-axis rate transducers   DART uses fluid as a part of its motion transduction mechanism. As most fluid-based inertial sensors, DART utilizes the law of conservation of momentum for fluid bodies. To clarify, DART sensors use a sphere of heavy liquid which rotated via a driver motor at high speed such that it would acquire high angular momentum. Across the contained fluid body, deflectable paddles are fixed along the circumference of the spherical cavity encapsulating the fluid. The paddles are connected to piezoelectric crystals, which act as the motion pick-off mechanism. However, a DART sensor is sensitive to angular rates along two mutually orthogonal axes, which are normal to the spin axis of the spherical cavity [4]. Figure 7 depicts a view of the internal structure of a DART sensor, from [4].

Jet flow and vortex rate gyroscopes   Jet flow gyroscopes measures the temperatures or pressure variations of a fluid body entrapped in container. Whereby, external angular rates cause variations in either temperature or pressure, which are measured, and are proportional to the applied angular rates [4].

Vortex rate gyroscopes use a container, where a 2-D sink flow is generated, which causes a vortex with a well-defined pattern of stream-lines. Whenever the sensor is t at rest, the vortex pattern remains unchanged. However, when the sensor is subjected to angular motion, the vortex pattern is changed in the form of an additional vortex being superimposed to the initial vortex pattern, which manifests as a combined vortex flow. The measurement of the fluid field velocities of the combined vortex flow would lead to the determination of the imposed angular rate to the sensor. Various designs have been reported for the concept of vortex rate gyroscopes [13–21].

Micromachined fluid-based angular rate sensors Micromachining of the fluid-based angular rate sensors have been attempted numerously. A micromachined biomimetic fluid rotor angular rate sensor was reported by Andreou et al. in 2014 to be used for vestibular prostheses [22]. It is noted that the vestibular system is the part of the human anatomy that is responsible for the detection of the head orientation in 3-D space. The vestibular system is a crucial for self-motion and body balance, adjusting body posture and helps stabilize the vision during movement [22, 23].

If one compares micromachined fluid-based inertial sensors to MEMS-based IMUs, it is found out that fluid-based inertial sensors utilize fluid instead of solid mass in their motion transduction mechanisms. Hence, they can have simpler structures and be at lower costs than respective MEMS-based inertial sensors. However, fluid-based sensors are limited in terms of sensitivity and bandwidth, when compared to MEMS-based sensors [24]. The concept behind those micromachined angular rate sensors are quite straightforward. Micromachined fluid-based angular rate sensors use either jet flow or thermal flow to measure angular velocities. For jet flow sensors, a micro pump is used to generate a laminar gas flow that is affected by external rotation of the sensor, and its disturbance is an indication of such rotation. Figure 8 shows schematic view of a uniaxial micromachined jet flow gyroscope, along with a diagram showing the jet flow with and without applied rotation, from [16].

Whereas, thermal flow angular rate sensors measure fluid flow because of thermal convection. Thermal gas gyroscopes utilize the same concepts used for thermal accelerometers, explained earlier. However, in a thermal gas gyroscope, the temperature sensors are mounted in a 2-D configuration to measure rotation rates instead of linear accelerations [24]. Figure 9 a schematic view of a thermal gas gyroscope, and the shape of the temperature profiles formed within the sensor before and after application of rotation rate, from [16].

Accelerometer technologies

The second constituent of an IMU is the accelerometer. Accelerometers are inertial sensors that measure the magnitude of an accelerating force, referred to as the
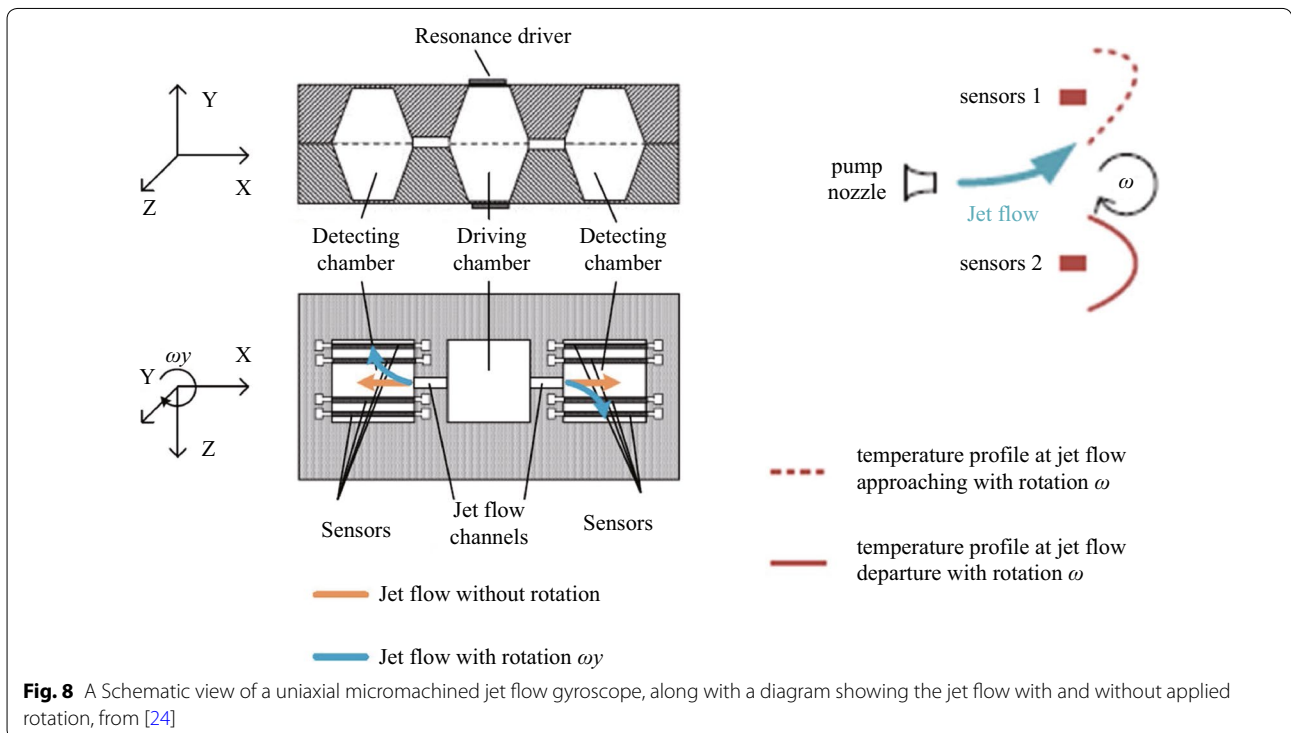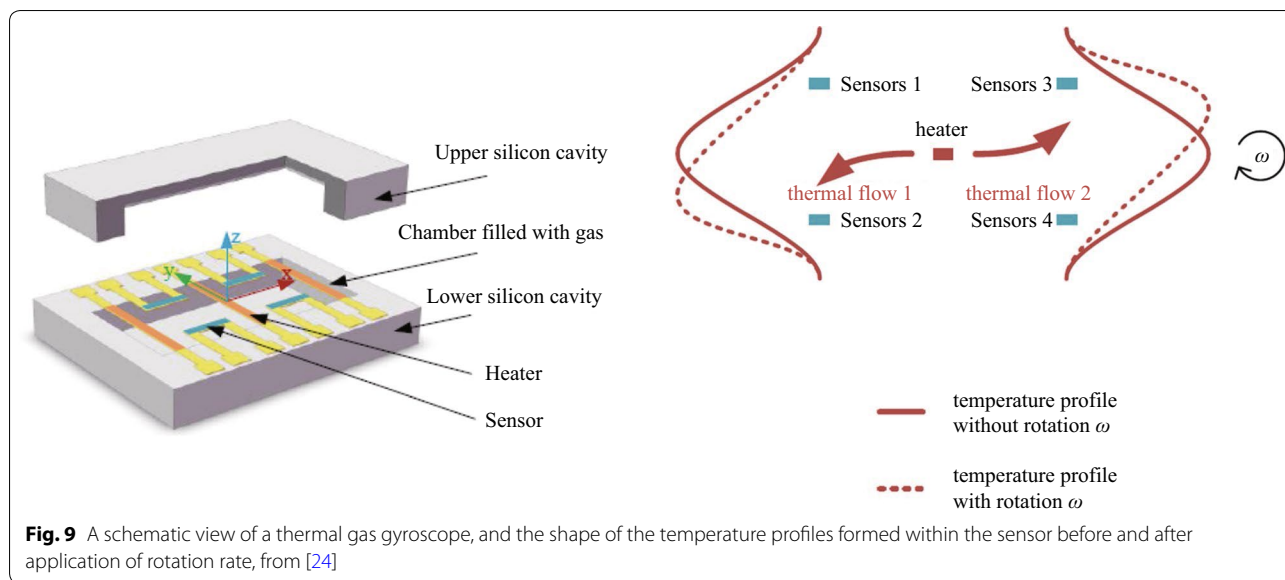

Fig. 8 A Schematic view of a uniaxial micromachined jet flow gyroscope, along with a diagram showing the jet flow with and without applied rotation, from [24]

Fig. 9 A schematic view of a thermal gas gyroscope, and the shape of the temperature profiles formed within the sensor before and after application of rotation rate, from [24]

specific force, as mentioned earlier in Sect. 0. It is noted that the inertial sensors industry is more mature in terms of accelerometers in comparison to the angular rate sensors. Nevertheless, state-of-the-art accelerometers include a huge variety of sensors which adopt different operation principles and technologies. State-of-the-art accelerometers include mechanical sensors which use the classical pendulum principle, up to the modern solid-state sensors. Consequently, accelerometers are found over a vast range of accuracies.

Mechanical accelerometers
Mechanical accelerometers can be considered of top tier in terms of accuracy as inertial sensors. Nonetheless, mechanical accelerometers can be realized in different forms with various designs. Mechanical accelerometers comprise a pendulum hinge mechanism, which is responsive to the applied linear acceleration. Such mechanical sensors are, in some cases, filled with fluid to enhance the damping effect within the sensor. Besides, the pendulum can be constrained to very small displacements, through implementing the sensor in closed-loop configuration, with a rebalance loop existent within the sensor design. Such closed-loop configuration aids in enhancing sensor accuracy and increases its input range. An example of such mechanical accelerometers are the force-feedback pendulous accelerometers [4]. Figure 10 shows a schematic 3D section of a force-feedback pendulous accelerometer, modified after [4].
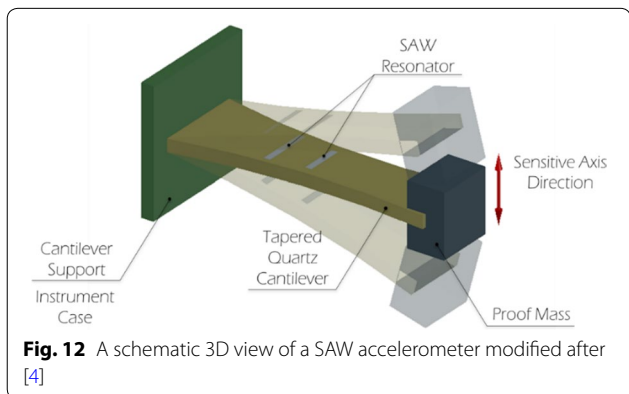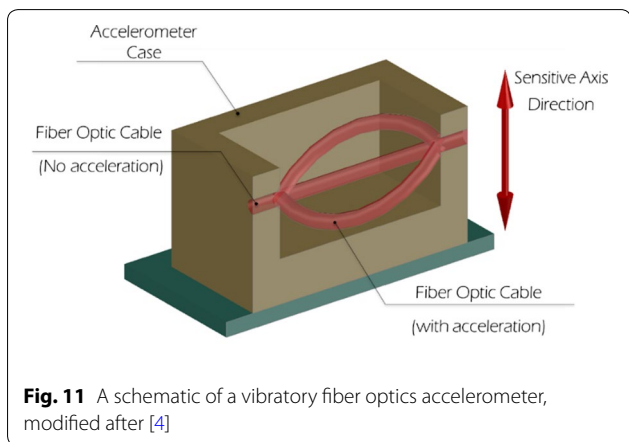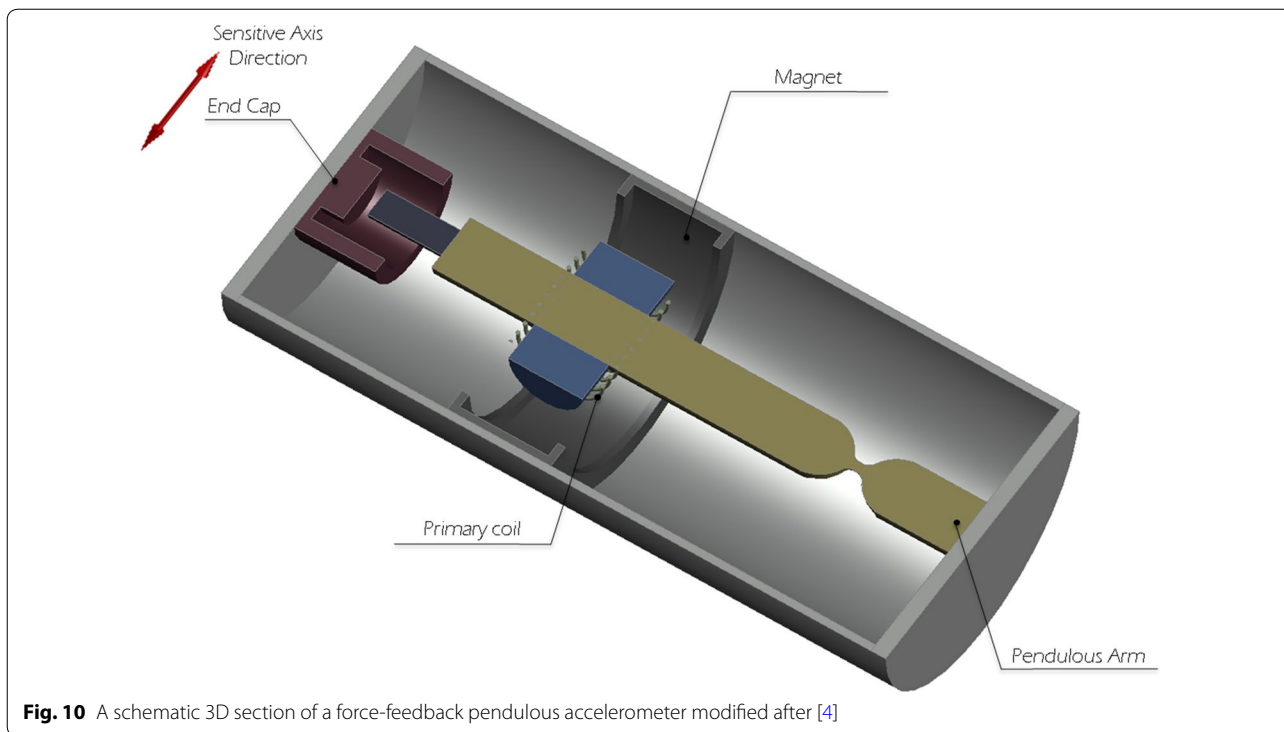
Another form of linear accelerometers are the accelerometers that utilize the solid-state technologies. Such accelerometers can be achieved by using various techniques including the use of vibratory devices, which is the case with vibrating quartz accelerometers, and silicon accelerometers [4]. It is noted that vibratory devices in accelerometers design provide the basis upon which MEMS-based accelerometers are fabricated.

Optical and surface acoustic wave accelerometers
Moreover, solid-state technologies include the realization of optical accelerometers, such as the vibrating fiber optics accelerometers [4]. Such optical accelerometers imply the use of fiber optics in the fabrication of the accelerometers and utilizes different approaches and designs to acquire the applied acceleration to the sensor from the measuring the light properties passing through various designs of fiber optics cables. Figure 11 shows a schematic of a vibratory fiber optics accelerometer. Another form of the sold-state technologies in manufacturing linear accelerometers if the surface acoustic wave (SAW) devices, which contains a pendulum hinge mechanism in the form of a cantilever beam to which a proof mass is attached; however, the pick-off mechanism in SAW accelerometers depends on the existence of a resonator on top of the cantilever beam, whose frequency is altered systematically as a function of any applied linear acceleration [4]. Figure 12 shows a schematic 3D view of a SAW accelerometer, modified after [4].

It is noted that solid-state technologies enable small, reliable, and relatively less expensive inertial sensors to be realized. Besides, it is states that sold-state technologies produce sensors that are mainly operated in an open-loop configuration. However, in some cases, closed loop design configurations can be attained using solid state technologies [4]. Table 3 shows a summary of typical

Fig. 10 A schematic 3D section of a force-feedback pendulous accelerometer modified after [4]

Fig. 11 A schematic of a vibratory fiber optics accelerometer, modified after [4]

Fig. 12 A schematic 3D view of a SAW accelerometer modified after [4]

performance characteristics for a range of accelerometers as per their underlying technologies, from [4].

Fluid-based accelerometers

For fluid-based linear accelerometers, the sub-categorization includes viscous float type accelerometers, pressure-driven accelerometers, and micro-machined thermal accelerometers.

Viscous float type accelerometers Viscous float type accelerometers rely on the concept of viscous drag and buoyant forces in a fluid medium and its interaction with solid bodies. Viscous float type accelerometers use a float placed within a chamber filled with a viscous fluid, as its sensing element. In a viscous float type accelerometer, the fluid filled chamber is usually rotated about the sensitive axis to provide a vorticity capable of lifting the solid float and keeping it buoyant within the swirling fluid. Whenever the sensor is subjected to an acceleration along its sensitive axis, the solid float is shifted within the chamber. The shift of the solid float is proportional to the input acceleration. Nonetheless, the shift of the float is detected using the pick-off mechanism of the sensor, which depends on the sensor design. Viscous float type accelerometers, themselves, are categorized into four types, depending on the type of pick-off mechanism utilized within the sensor design. Viscous float type accelerometers can be inductive, capacitive, photo-electric, and variable resistance

Table 3 A summary of typical performance characteristics for a range of accelerometers as per their underlying technologies, from [4]

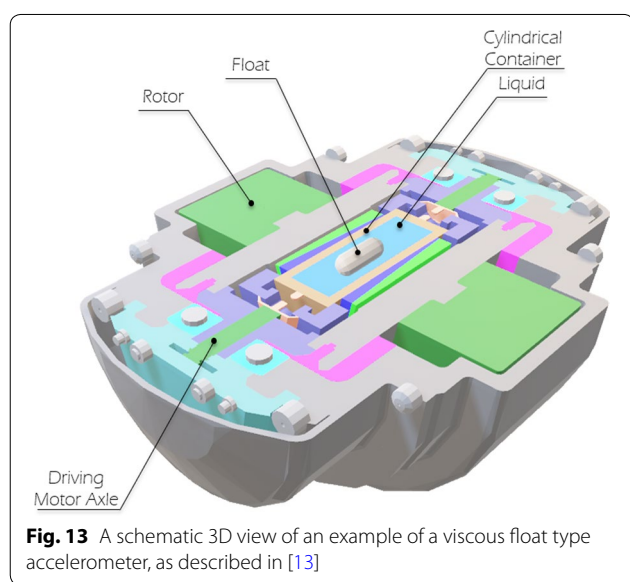| Characteristic	Accelerometer type				
	Force-feedback pendulous	Vibratory fiber optic	Vibrating quartz	SAW	Silicon
Input range (g)	±100	±20	±200	±100	±100
Scale-factor stability (%)	0.1	0.001	0.01	0.1–0.5	0.5–2
Scale-factor non-linearity (% full scale)	0.05	0.05	0.05	<0.1	0.1–0.4
Fixed bias (mg)	0.1–10	1	0.1–1	<0.5	<25
Threshold (μg)	10	1	<10	1–10	1–10
Bandwidth (Hz)	400	100	400	400	400

Fig. 13 A schematic 3D view of an example of a viscous float type accelerometer, as described in [13]

accelerometers [25–32]. It is noted that viscous float type accelerometers are found in both open-loop and closed-loop design configurations. The common limitation of viscous float type accelerometers is being affected with the thermal variations which have huge impact on the fluid viscosity, which affected the sensor output. Figure 13 shows a schematic 3D view of an example of a viscous float type accelerometer, as described in [31].

Pressure-driven accelerometers Another form of fluid-based linear accelerometers was introduced by Schmidlin [33], and is referred to hereafter as pressure-driven linear accelerometer. The sensor was designed as an open-loop system, where the sensor was designed to not have a feedback mechanism, as the sensor does not contain a proof mass to detect the linear acceleration to which it is subjected. The scientific concept behind the sensor design is to use the differential hydrostatic pressure created on a fluid charge entrapped within a container as a direct measure of the linear acceleration. To clarify, it is known that from the Navier–Stokes equations that the pressure gradient along with the viscous forces should be in equilibrium with the external inertial force imparted to the fluid. Consequently, if one manages to measure the pressure gradient, for a constant viscous force, the linear acceleration can be computed thereafter from the Navier–Stokes equations. However, the reported invention just uses an analogy derived from Navier–stokes equation, where it is postulated that linear acceleration is directly proportional to the generated pressure gradient.

Nonetheless, the sensor basic internal structure constitutes a porous cylindrical container, which can be made of porous ceramics or sintered powdered metal compacts. The porous container in filled with a charge of non-wetting heavy liquid, such as mercury, metal liquid, or the like. The non-wetting liquid is designed, such that it does not fill the entire porous cylindrical container. The porous container is sealed on both its bases by two endcaps, which share an intricate design. Each end cap is designed to have a means of gas inflow that is connected to a plenum fitted therewith. The plenum is then connected to the non-wetting liquid through a series of passages, and orifices. It is noted that gas inflow means has a series of filters, valves, and inlet metering orifices to keep track of the mass flow rate being diffused through the system. Besides, the gas plenums are also provided with gas outflow orifices, which are connected externally to a set of pressure manometers to measure the pressure differences. The pressure manometers are arranged, such that there is a pressure manometer that is connected to both gas outflow orifices from both end caps. Whereas, there are other two pressure manometers, where each is connected to one of the end caps, with their other branches subjected to atmospheric pressure to measure the absolute pressure of the gas within each end cap. The series of pressure manometers represent the pick-off mechanism of the sensor.

When the pressure-driven accelerometer is stationary, as constant gas flow rate is pumped through the gas inflow means through the endcaps, and to the non-wetting fluid, where the excess volume of gas is being diffused out of the sensor through the porous walls of the cylindrical container. In such case, the pressure at both end caps is equal; hence the pressure gradient is equal to zero, and the accelerometer theoretically reads zero-acceleration output.

On the other hand, when the pressure driven accelerometer is subjected lo linear acceleration along its sensitive axis, which is an axis parallel to the longitudinal axis of the porous cylindrical container, the liquid charge tends to follow the law of conservation of momentum. Consequently, pressure builds up on one endcap, and reduces at the other endcap. This difference in pressure would affect the pressure by which the gas is pumped into the system, and which is monitored by the pressure manometers. To clarify, the end cap that experiences elevated pressure for the gas outflow due to motion is going to register high absolute pressure value through the connected manometer. Whereas, on the other hand, the other end cap would register a lower absolute pressure value for the gas outflow. Consequently, the generated pressure difference between both endcaps can be measured using the differential pressure manometer and double-checked by the two absolute pressure manometers. Consequently, the linear acceleration can be computed depending on the proportionality with pressure difference. Figures 14 and 15 show a schematic 3D view of the pressure-driven accelerometer with its reported pick-off mechanism in [33]. However, there other designs for pressure driven accelerometers as reported in [30].

Micro-machined fluid-based accelerometers Micro machined accelerometers represent a different form of fluid-based linear accelerometers. The micro-machined thermal accelerometers operation principle is based on the free-convection heat transfer of a tiny hot air bubble in an enclosed chamber. The sensor comprises a heater that is placed at the center of chamber. The heater is operated at high joule power. Adjacent to the heater, two temperature sensors are placed, one at each side of the heater. The temperature sensors are designed to operate at low joule power. The temperature sensors are either built as thermistors or thermopiles. A gas fills the chamber that contains the heater and the temperature sensors.

When the sensor is stationary, the heater heats the entrapped gas, and lowers its density. In such case, free convection is induced, and builds a temperature profile that is symmetrical, such that the two temperature sensors read the same value. However, when the sensor is
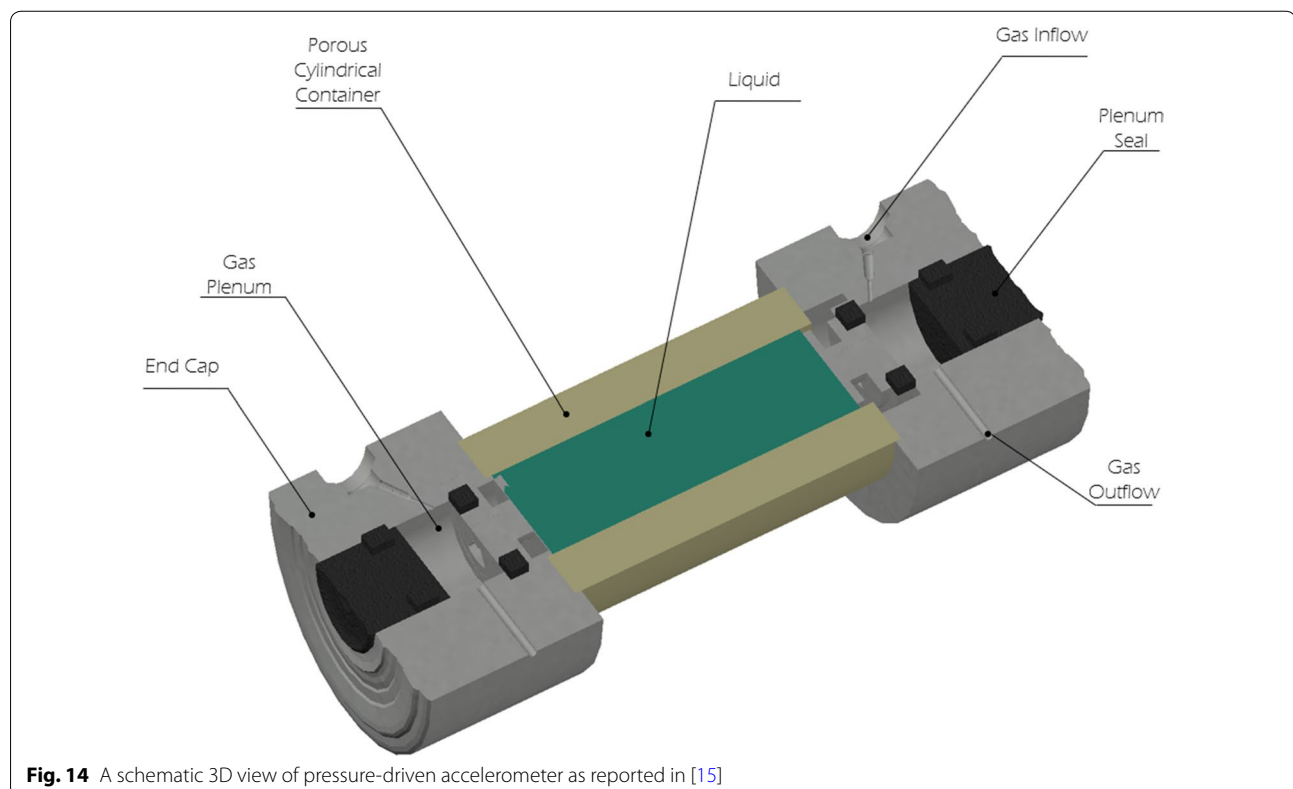

Fig. 14 A schematic 3D view of pressure-driven accelerometer as reported in [15]

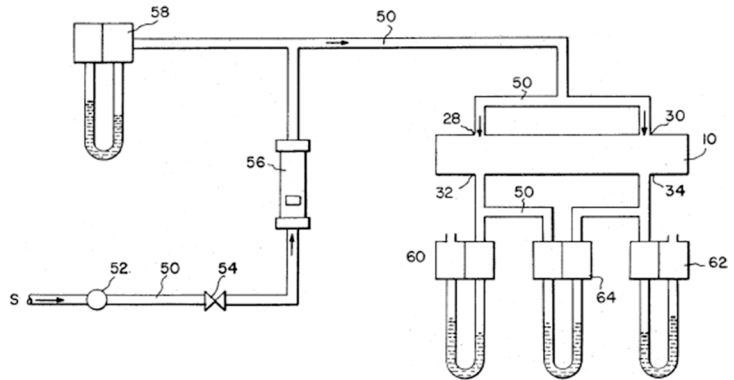| No.	Element Identification
10	Sensor Main Body – See Figure (5)
28,30	Gas Inlet Orifices
32,34	Gas Outlet Orifices
50	Conduit System
52	Gas Filter
54	Valve
56	Rotometer
58	Pressure Manometer – for Inflow Gas
60	Absolute Manometer – Outflow Gas @ 32
62	Absolute Manometer – Outflow Gas @ 34
64	Differential Manometer – Outflow Gas 32,34

Fig. 15 The reported pick-off mechanism for a pressure-driven accelerometer, from [33]

subjected to lateral acceleration, the temperature sensors read different values. Hence, the temperature profile is deflected towards a direction opposing to the direction of the applied acceleration. Nonetheless, the temperature difference is fed into a conditioning circuit which generates and electric signal that is proportional to the applied acceleration.

The first thermal convective single axis accelerometer was introduced by Leung et al. in 1997 [24, 34]. However, a dual axis version of the sensor was introduced by Leung et al. in 1998 [24, 35]. The sensor followed the same operation concept, and motion transduction mechanism. However, instead of using a pair of thermal sensors, the dual axis thermal accelerometer utilized four thermal sensors that are placed on two orthogonal axes in a common plane. Hence, the sensor can sense accelerations along two orthogonal axes. Advancements were made to this form thermal accelerometers to try and enhance their performance. Attempts have been made to reach a monolithic triaxial thermal accelerometer. A triaxial

thermal accelerometer was introduced by Leung et al. in 2011, which constituted a buckled cantilever assembly upon which the heaters and sensors are mounted [36]. Figure 16 shows a schematic view of a uniaxial thermal gas accelerometer, along with the form of the temperature profiles as measured by the deployed thermal sensors before and after motion, as depicted in [16].

Future trends in inertial sensors technologies

This section provides a summary of the future trends in inertial sensor technologies, and the recent advancements occurring in designing and fabrication of inertial sensors of lower cost, higher performance, and smaller in size, in comparison to current state-of-the-art inertial sensors. The advancements in inertial sensor technologies would enable the use of inertial navigation in a wide area of applications.
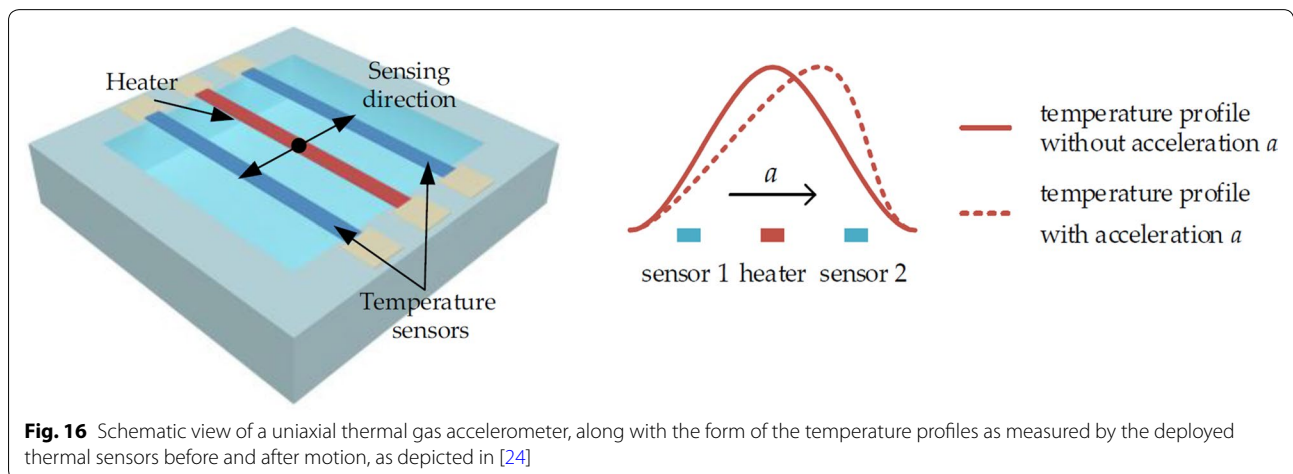
Fig. 16 Schematic view of a uniaxial thermal gas accelerometer, along with the form of the temperature profiles as measured by the deployed thermal sensors before and after motion, as depicted in [24]

Nuclear magnetic resonance gyroscopes

The physical phenomenon governing the operation of nuclear magnetic resonance (NMR) gyroscopes is the quantum spin of atoms nuclei [2]. In quantum mechanics, it is well-known that many atoms exhibit a property referred to as nuclear spin. A nuclear spin entails that a nucleus, of a given atom, acts as if it were spinning. This is the case in most atoms with odd mass, odd atomic number or both [37]. However, the property of nuclear spin do not occur for atoms with even mass number or atomic number or both. These atoms are characterized by having quantized spin angular momentum and magnetic moment, which is calculable. The relevant aspect of the nuclear spin is that the nuclear spin is affected under the impact of external magnetic field. Hence, one can drive a transition between different spin states by applying radio-frequency electromagnetic radiation [38].

To clarify, the nuclear spin is an indication of the total angular momentum of the nucleus. Although, the nucleus is composed of neutrons and protons, it acts as a single entity with an intrinsic angular momentum, which is the nuclear spin. The nuclear spin is dependent on the mass number of the atom.

Consequently, if the nuclear spin could be affected by the externally applied electromagnetic radiation, the nuclear spin could be polarized, and some how the nuclear spin states could be manipulated. Hence, it has been concluded that a spin polarized nucleus will precess at a certain frequency when subjected to a magnetic field. The precession frequency is known as Larmor frequency and depends on the atom whose spin is polarized, and on the magnetic field applied to the atom [38]. Nonetheless, the rotation of a cell containing spin-polarized-nuclei will modify the precession frequency proportional to the applied angular rate.

NMR gyroscopes have reached considerable development in major aspects of its design and implementation. Specifically, research advancements have led to enhanced method of controlling the atomic spin, applied magnetic field, and the development of better pick-off mechanisms to record the gyroscope signal.

It is stated that NMR gyroscopes approaches navigation requirements in terms of error budget [39]. Besides, NMR gyroscopes are unaffected by vibrations because of the motion transduction mechanism of such sensors, which do not require a solid proof mass. To sum up, NMR gyroscope technology is expected to reach high levels of accuracy in high dynamic applications within a decade [2].

Cold atom inertial sensors

Another recent technology that has been implemented in inertial sensors fabrication is cold-atom technology. The cold-atom inertial sensors rely on laser cooling of atoms, without cryogenic cooling. To clarify, subjecting the atoms of some materials to laser beams at frequencies close to the atomic resonance of said materials would trap atoms. Thus, the atoms would lose their kinetic energy and drive their temperatures to micro-Kelvin ranges [2].

Consequently, the trapped atoms would show some quantum mechanical behaviours, such that their states could be altered with various techniques. The trapped atoms could be manipulated by the application of tuned laser pulse and letting the atomic wavefunctions interfere after moving along a designated path in space [40], in a similar way to that way in which FOG operates; however, instead of using light waves, the atomic wavefunctions are used.

Other than implementing the cold-atom technique in a similar way of interfering wavefunctions (as mentioned above), there are various ways to implement the cold-atom technique for inertial measurements. One way is that if the trapped atoms are released from the laser cooling, they would act as free-falling masses. Afterwards, the acceleration of the inertial sensor case can be measured relative to these atoms. However, other approaches have been implemented to manipulate the trapped atoms and use them inertial measurements. It has been reported that the atoms can be set to a fixed velocity or can be guided for acceleration ad rotation measurements [41].

Nevertheless, cold-atom inertial sensors are characterized of having high performance in comparison to typical optical gyroscopes, because the effective atom wavelength is less than that of RLG of FOG by ten orders of magnitude. Additionally, due to low temperature of the trapped cold atoms, they provide low noise measurements and high signal to noise ratio (SNR) relative to optical inertial sensors [2].

Micro-opto-electro-mechanical-systems (MOEMS) inertial sensors

In contrast to MEMS-based inertial sensors, which utilize capacitive pick-off mechanisms, a new approach emerged known as micro-opto-electromechanical systems (MOEMS). MEMS-based IMUs usually include an electronic capacitive means by which the motion of the micro inertial seismic mass is detected and transformed into signals. However, MOEMS-based inertial sensors utilize optical pick-off mechanisms which eliminate a vast range of errors that occur in MEMS-based sensors.

Various pick-off mechanisms have been introduced and researched. According to [4], the optical pick-off mechanisms are classified into interferometric approaches or attenuation approaches. The interferometric pick-off mechanisms utilize similar concepts applied in FOG,

which offer low noise and high-resolution inertial sensors. On the other hand, attenuation pick-off mechanisms use means to interrupt the light beam from a diode.

Additionally, the optical pick-off mechanism is also researched for optimizing the installation and harmonization of the optical source (i.e., light source) and its detector. Nonetheless, MOEMS sensors are also optimized to achieve low-cost manufacturing while achieving high accuracies [42–44].

Particle imaging velocimetry inertial sensors

Recently, a fluid-based inertial sensors technology is being developed by the Mobile Multi-sensor Systems research group at the University of Calgary. The research proposes a fluid-based inertial navigation system, referred to as particle imaging velocimetry inertial navigation system (PIVINS), depends on fluid dynamics to provide the inertial measurements. The concept is that when an inertial force is imposed upon a control volume of fluid, a flow is generated in response to such force in order to satisfy Newton's second law of motion. Hence, once the flow can be detected, and through the implementation of fluid dynamics theories, the actual inertial measurement can be acquired. The fluid dynamics theories, which are of interest to design this system, are the law of conservation of momentum implemented for incompressible fluids, or alternatively referred to as Navier–Stokes equations, and the continuity equation for an incompressible fluid. The concept is applicable for either linear or rotational types of motion.

From the proposed nomenclature, PIVINS employs a version of particle imaging velocimetry to perform the inertial measurements. Particle Imaging Velocimetry is a branch of fluid dynamics science in which the properties of fluids and fluid flows can be determined through tracking particles that are neutrally buoyant, which mimic the actual dynamics of the flow. Particle imaging velocimetry implies the use of an imaging sensor that are used to track the particles, whether those imaging sensors are set up in fixed or moving positions along the examined flow. Research has been extensive in particle imaging velocimetry with vast technical advancements in digital image processing to acquire more precise, computationally efficient, and high rates of data.

However, in this adoption of the concept within PIVINS, only one particle is monitored within a predefined control volume flow channel, and the particle monitoring is done using a fixed imaging sensor with respect to the pre-located and fixed flow channel. The motion of such particle is determined from the acquired sequence of images via a series of digital image processing techniques.

PIVINS consists of two triads of fluid flow channels place along 3 mutually orthogonal planes, with an imaging sensor that is facing each plane to track a particle that is placed in each flow channel. One triad represents a set of orthogonal gyroscopes, and the second triad represent the accelerometers. The particles are chosen to be of the same density of the fluid filling up the flow channels to be neutrally buoyant.

Two patents have been filed and are currently pending, and research is currently ongoing to reach a fully functional inertial navigation system [45, 46]. The PIVINS is nearly a drift-free inertial navigation system with minor bias instability. Whereby, The PIVINS endures only systematic errors that can be modeled either analytically or experimentally. Hence, the PIVINS is comparable at each level to a high-end tactical grade IMU, and yet extremely efficient in terms of bias instability. It is expected that the PIVINS reaches such level of performance with a simple low-cost design.

Hemispherical resonator gyroscope technology

Hemispherical resonator gyroscope (HRG) technology follow the same underlying scientific principles implemented in vibratory gyroscopes, as discussed earlier. The HRG depends on Coriolis force in detection of input angular rate. Hence, HRG technology lies within the more specific taxonomy of gyroscopes, which is referred to as Coriolis Vibratory Gyroscopes [47]. The underlying scientific principle states that a supported resonating object at a given frequency would remain resonating along the same plane even if its supports are rotated.

Typically, an HRG includes a hemispherical dome resonator of a piezo-electric material as an inertial sensing element that is resonated at a predetermined frequency generating a standing wave across the hemispherical dome [4]. HRG utilizes a piezo-electric (for example: quartz) which senses the locations of the nodes and antinodes of the standing wave pattern of the hemispherical resonator. To clarify, the pick-off mechanism utilizes a series of pick-off electrodes that are placed across the outer circumference of the resonator. The electrodes and the resonator act as a series of capacitors that produce capacitive electrostatic charges between the metal coated surfaces on the quartz components. Another use of the pick-off electrodes is to sustain the standing wave pattern. Besides, the resonator driving mechanism, which takes the form of a forcer electrode ensures that hemispherical dome resonates at a specific frequency. Figure 17 shows a schematic of the HRG main components and main operation concept, as found in [4].

When the HRG is stationary, the sensor is designed such that the resonator generates a standing wave whose

nodes are located midway between the successive pick-off electrodes, as shown in Fig. 17. However, when a rotation is applied to the HRG a tangential force develops due to the generated Coriolis acceleration, which could cause the standing wave pattern to shift along the circumference of the resonating hemispherical dome, as shown in Fig. 17. In such case, the shifted standing wave pattern is rotated at a precession angle with respect to the stationary standing wave pattern. The precession shift angle is proportional to the input rotation rate.

The main advantages of the HRG design over other CVGs lies within some key aspects. The HRG ha a resonator that is axisymmetric about the sensor's rotation axis. Such setup ensures optimal decoupling between the resonator and the outer world. This can be achieved when the resonator's support is placed at a vibration node of the generated standing wave pattern. Besides, the resonating flexural waves are controlled by electrostatic forces, which minimizes the requested energy and minimizes the errors induced by the electronics imperfections. Additionally, the topology of a hemispherical dome enables each gram of the resonator to flexural energy storage, in comparison to other CVG resonators. Moreover, the hemispherical resonator is made of amorphous fused quartz for optimal isotropy and minimizing energy dissipation. Finally, the metallic coating of the electrodes ensures minimal energy dissipation within the electrodes.

The HRG technologies was first developed in the 1980s by Delco (now the Northrop–Grumman Corporation, Litton Systems) [4, 48]. Their HRG sensors has 58 mm resonator diameter and had a bias instability 0.0001 °/h, scale factor accuracy less than 1 ppm, and an angular random walk of 0.0008 °/√h.

Afterwards, attempts have been made to scale down the size of the HRG to be suited for bore hole applications. Besides, the HRG needed to be accommodate mechanical shock and vibration [49]; however, the results did not meet the cost requirements for mass production of HRG. Whereas, attempts have been made in Russia to achieve HRG, which have reported an HRG of 30 mm resonator diameter [50].

Recently, SAFRAN, a leading international corporation specializing in aerospace, aviation, guidance and navigation applications, have developed a new HRG design that ensures achieving a gyroscope of higher performance, smaller size and a lower cost. The SAFRAN HRG design is advantageous over its predecessors due to some optimizations and enhancements that SAFRAN have
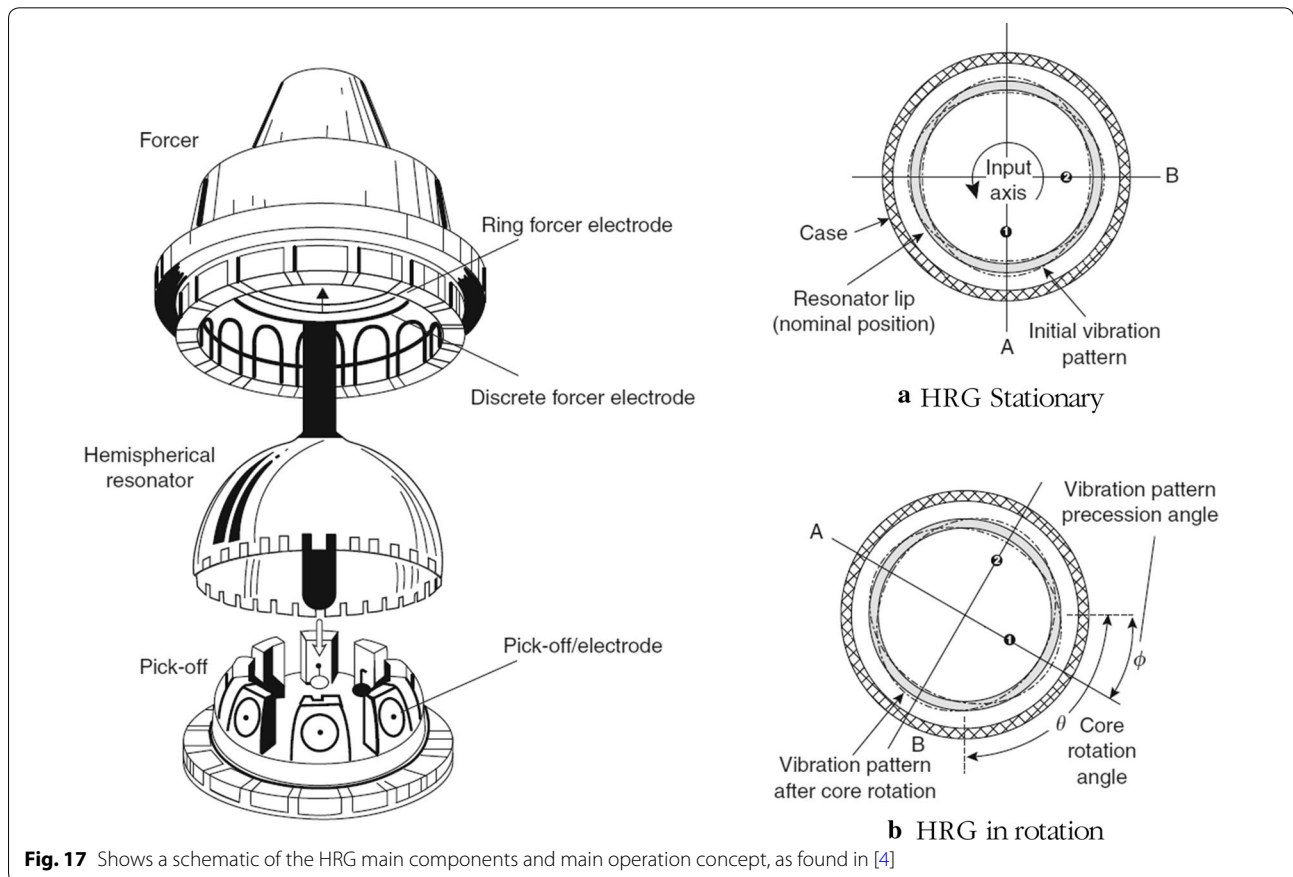

Fig. 17 Shows a schematic of the HRG main components and main operation concept, as found in [4]

implemented to the scientific operation principle of the HRG.

SAFRAN exploited the fact that the performance of an HRG does not depend on the size of its resonator. Rather, the performance of the HRGs depend on the Q-factor and the quality of how the flexural standing waves are driven. Besides, they have found a solution to the major drawback of the HRG, having high manufacturing costs. The high manufacturing costs of the HRG result from the requirement of the high precise manufacturing and assembly of the sensor [47].

Therein SAFRAN introduced their patented electrodes support design that ensures that the resonator driving forces are generated at the equatorial plane of the hemispherical dome such that the assembly of the resonator is only crucial along the 2D equatorial plane [47, 51]. Hence, the resonator becomes isotropically gapped from the standing flexural wave driving electrodes.

SAFRAN's HRG reached a size of 20 mm resonator at low cost that can satisfy the demand of the mass market. SAFRAN claims that their HRG can replace optical technologies such as FOG and RLG and even replace Cold Atom technology, as well. SAFRAN's HRG has been implemented and tested for various applications including but not limited to: strategic, navigation and tactical grade IMUs, cost -effective marine compasses, tripod mounted north finders, space launchers, INSs for commercial aircrafts, weapons guidance systems.

Such applications could only be fulfilled by sensors of extremely high performance. As per SAFRAN, their HRG is reported to have angular random walk 0.0002 $°/\sqrt{h}$. Besides, SAFRAN have not reported a specific value for the bias stability of their HRG on account of the requirement of a longer testing time for Allan Variance to provide a proper estimate of the bias stability value. However, SAFRAN projected the bias instability value to reach 0.0001°/h as root mean square error (rms) over 2000 h test period.

There are various aspects that are open for intensive research, as reported by SAFRAN [47]. Such research aspects include: bias stability optimization, enhancement of control electronics of the HRG and the implementation of more adequate calibration and compensation models.

Inertial sensors performance

As stated earlier, inertial sensors are categorized, as per their performance, into different grades which are separated by their respective costs, and suitable applications. The basis upon which IMUs classifications are built are the errors that occur within their output measurements. Such errors vary between inertial sensors in terms of their nature being systematic or random errors.

Moreover, inertial sensor errors vary as per their sources, which is mainly attributed to their operation concept and their underlying technologies. Additionally, such errors affect the classification of the IMUs as per magnitude within the inertial sensors' measurements.

Consequently, inertial sensors errors can be, in some sort, a measure for the sensor performance. Hence, such errors, or performance measures, provide a basis of comparison between inertial sensors technologies. Nevertheless, all inertial sensors share a common ground of discrepancies that are inevitable.

The institute of electrical and electronics engineers (IEEE) have published a standard for inertial sensor terminology that include the scientific definitions for terminologies that are encountered, when studying inertial sensors operation [52]. Nonetheless, the standards provide a set of definitions to the most common inertial sensor performance measures. These performance measures are grouped hereafter to provide a basis upon which inertial navigation technologies, that are discussed afterwards, are evaluated. Interested reader is referred to the IEEE standards document [52] for complete definitions of said performance measures.

Stochastic error modeling for inertial navigation

Inertial navigation systems provide high accuracy navigation states over short time intervals. The high-accuracy navigation solution is function of the grade of the utilized IMU. Nonetheless, whenever the operation period of IMUs increase, the error budget within the acquired navigation solution increases as well. Hence, to acquire an accurate navigation solution from an INS, the stochastic errors within the included inertial sensors must be modelled.

Generally, random errors, within inertial sensors, are all modeled as random processes within the navigation solution scheme whenever the inertial measurements are integrated with an update source to end up with an error bounded navigation solution [1]. However, the model determination of a certain random process to be included into a navigation algorithm encompasses a major research aspect in inertial navigation. There are various methods by which the stochastic errors of inertial sensors can be characterized and mathematically model. This section gives a brief discussion of the most effective methods of modeling inertial sensor errors.

Autocorrelation function method

As mentioned above, the inertial sensors random errors are incorporated into navigation filters (e.g., the Kalman filter) as random processes. The random processes are expected to describe how the inertial sensor errors evolve over time. Therefore, it is crucial to accurately determine

the parameters of the chosen random processes that are used to describe the inertial sensors errors. Otherwise, the estimation algorithm would yield inaccurate navigation solution, which would grow even less accurate over time.

Consequently, it is a major aspect of performing navigation applications to better describe the inertial sensors error terms and include them in the navigation filter to be implemented. One of the most popular methods in estimating the stochastic errors in inertial sensor measurements is deducing the autocorrelation function (ACF) for the inertial sensor error signal.

The stochastic errors of inertial sensors are typically characterized by being correlated over time [1]. This is the reason behind modeling the stochastic inertial errors as random processes. Besides, as a general assumption, the inertial sensor errors are assumed to be stationary processes, which implies that the statistical properties of the error signal of any given inertial sensor would be the same over time [53]. The most common random process which are considered when using the ACF method is the 1st order Gauss Markov. Whereas, most inertial sensor stochastic errors are assumed to follow a 1st order Gauss Markov process.

When one computes the ACF of any given inertial sensor error signal, the underlying time-correlated low frequency random process could be deduced. Moreover, the parameters that could describe such random process (usually, 1st order Gauss-Markov process) could be easily acquired from the auto-correlation sequence.

To compute the autocorrelation function of experimental inertial data, a substantially long period, which could reach 8 h, of inertial sensor data is acquired in a well-known controlled environment. The acquired inertial measurements should have extremely accurate reference values. Hence, it is usually recommended to acquire long periods of inertial measurements while the sensor is stationary in a laboratory environment. Afterwards, to get rid of the high frequency noise, which inversely occur over short period of time, denoising is implemented using wavelet denoising. It is noted that the level of wavelet denoising should be considered not to affect the required sampling rate for the respective inertial navigation application for which the inertial sensors are intended. The detailed method of deriving the ACF for inertial measurements is provided in [53].

In some instances, the power spectral density (PSD) function is drawn instead of the autocorrelation of the inertial error time series. However, the PSD only represents the Fourier transform (FT) of the autocorrelation function. Consequently, the drawn information about the stochastic error parameters should coincide from using wither approaches to acquire them [53].

Nonetheless, the ACF endures some drawback when it comes to implementation. The common practice in inertial navigation is that the random process parameters, which are deduced based on ACF are usually non-optimal and require some tuning when being used in navigation filters. Besides, ACF method would render itself inadequate when used for modeling inertial sensor errors in high dynamics applications, or for higher order random processes. On the other hand, when using the PSD method, it had been found to be sufficient for high frequency noise processes, such as White Noise. However, PSD lacks accuracy when it comes to determining the low frequency noise parameters [54].

Allan variance method

There have been several variance techniques that could be used for stochastic modeling of errors in inertial sensors. The simplest of those techniques is the Allan variance, reported initially in [55]. The Allan variance method utilizes the root mean square (RMS) random-drift error as a function of averaging time. For a detailed description of the derivation of the Allan variance, the reader is referred to [55, 56]. However, by computing the Allan deviations across the entire length of data, a characteristic curve is acquired, which is usually represented in a log–log scale, showing the averaging time versus the Allan deviation values. By further examining the characteristic curve, one could discern the major error components within the acquired inertial sensor data.

Allan variance can be used to identify the underlying stochastic errors that could occur in the read-out signals of inertial sensors. Besides, Allan variance provide the capability of classifying the stochastic error components. To be specific, the Allan variance method can characterize five stochastic error terms that occur in inertial sensors measurements, which are: the quantization noise, the random walk, the white noise, bias in-stability, and rate ramp [57].

Nevertheless, once the Allan variance is computed for the different error terms, the acquired Allan variance can be utilized through different models to compute the parameters that could better represent the random process that could be incorporated into a navigation filter. Besides, the Allan variance provide information on the type and magnitudes of various error terms. The Allan variance method has been used to identify and characterize the stochastic error components in various inertial sensors of different grades, as reported in [49, 50].

However, the main drawback of the Allan variance method is being statistically inconsistent in modeling stochastic errors in small and low-cost MEMS-based IMUs [54].

Generalized model of wavelet moments (GMWM) method
The generalized model of wavelet moments (GMWM) method is a statistical method that has been utilized recently for inertial sensors stochastic error modeling. It represents a futuristic trend in inertial sensor error modeling techniques. However, the GMWM method was introduced initially in [58].

The GMWM is an estimation method which utilizes the Generalized Method of Moments by using the wavelet variance (WV) as an auxiliary parameter [54, 59]. Whereby, the GMWM utilizes the relation between the WV and the parameters of random processes, to be included in stochastic model, to estimate the latter by minimizing the distance between the empirical and model-based WV. Interested readers are referred to the detailed description of the GMWM method for inertial sensors error modeling in [58]. However, it is noted that the random processes that are commonly encountered within inertial sensor measurements, and which are found extensively in literature are: the quantization noise, white noise, auto-regressive process of 1st order, and drift ramp, as shown in [54]. Additionally, in most cases the 1st order auto-regressive process could be transformed mathematically into 1st order Gauss-Markov process.

Additionally, enhancements have been made for the GMWM model to better model the stochastic error terms of low-cost inertial sensors. Such enhancements include the used of Multi-signal GMWM method. To clarify, the need for the Multi-Signal GMWM arises from the fact that the GMWM method assumes a stationary process when it comes to the nature of the error signal acquired from a given inertial sensor. However, this is assumption becomes unrealistic when trying to handle stochastic errors of low-cost MEMS-based IMUs. Consequently, the Multi-signal GMWM provides an approach to overcome the stationarity assumption and enables handling non-stationary inertial error signals. Further explanation and discussion of the method can be found in [54].

Nevertheless, The GMWM method has been proven effective and advantageous over typical methods including the Allan variance method in terms of its accuracy in characterizing the inertial sensors error components and the computed parameters are more suitable for direct implementation in navigation filters.

Summary
In this review paper, inertial navigation technologies have been broadly covered. Nevertheless, it has been shown that the inertial navigation technologies have significantly matured. Whereas, inertial sensors have been developed enough to meet the high-accuracy demand of broad navigation applications. Hence, the INSs have transformed from being bulky in size and high in cost into reliable, small, and low-cost systems, that could be utilized for high accuracy navigation applications. Besides, future trends in inertial navigation technologies, which are under continuous development, provide considerable promise in terms of the achievable size, weight, power consumption, and accuracy. Ergo, INSs could be extended to further applications with high reliability and accuracy even without the availability of aiding or fusion with other navigation systems such as GNSS.

Furthermore, a brief overview has been introduced on state-of-the-art techniques that are being used to model the stochastic errors of inertial sensors, that are intended to be used in inertial navigation applications. It has been shown that accurately modeling the inertial sensors stochastic error components could significantly improve the navigation solution acquired from said inertial sensors for longer periods of unaided operation. Furthermore, the method of GMWM has been introduced, which represent a futuristic trend stochastic error modeling technique. With further enhancements being introduced to the GMWM method, it is expected to have better stochastic models that could better characterize the inertial sensors errors and provide more accurate navigation solutions in stand-alone operation mode of the INSs.

To sum up, vast research achievements have been made into using extremely low-cost inertial sensors in navigation applications and the error modeling of said sensors. This research endeavors aim at having higher accuracy navigation solution with the use of extremely low-cost sensors in accuracy-critical navigation applications including oil ang gas industry, aerospace navigation, pedestrian dead-reckoning (PDR), wearable devices, indoor navigation applications, unmanned aerial vehicles (UAVs), and self-driving cars.

References

1. Noureldin, A., Karamat, T. B., & Georgy, J. (2013). *Fundamentals of inertial navigation, satellite-based positioning and their integration* (1st ed.). Berlin: Springer.
2. Tazartes, D. (2014). An historical perspective on inertial navigation systems. In *2014 international symposium on inertial sensors and systems (ISISS)*, pp. 1–5.
3. Groves, P. D. (2015). Navigation using inertial sensors [Tutorial]. *IEEE Aerospace and Electronic Systems Magazine, 30*(2), 42–69.
4. Titterton, D., & Weston, J. L. (2011). *Strapdown inertial navigation technology* (Vol. 17). London: IET.
5. Beckwith, T. G., Buck, N. L., & Marangoni, R. D. (1982). *Mechanical measurements*. Bostoon: Addison-Wesley Pub. Co.
6. Passaro, V. M. N., Cuccovillo, A., Vaiani, L., De Carlo, M., & Campanella, C. E. (2017). Gyroscope technology and applications: A review in the industrial perspective. *Sensors, 17*(10), 2284.
7. Pittman, R. (1967). *Rate integrating gyroscope*. 3,359,806. December 26, 1967.
8. Zeldman, M. I., & Feinberg, R. (1966). *Fluid rate-integrating gyro*. US3261213 A. July 19, 1966.
9. Lahde, R. N. (1960). *Integrating rate gyroscope*. US2951377 A. September 06, 1960.
10. Diamantides, N. D. (1968). *Rate gyroscope*. US3367194 A. February 06, 1968.
11. Summers, T. O. Jr. (1960). *Rate integrating gyro*. US2951375 A. September 06, 1960.
12. Huvers, M. E. (1978). *Rate integrating gyroscopic aiming method and device therefor*. US4087919 A. May 09, 1978.
13. Ogren, H. D. (1965). *Vortex rate sensor*. US3203237 A. August 31, 1965.
14. Senstad, P. D. (1966). *Magnetically and electrically rebalanced vortex rate sensor*. US3230765 A. January 25, 1966.
15. Barrett, D. (1966). *Vortex rate sensor*. US3240060 A. March 15, 1966.
16. Camarata, F. J. (1969). *Twin vortex angular rate sensor*. US3447383 A. June 03, 1969.
17. Sieracki, L. M. (1969). *Vortical comparator*. US3452768 A. July 01, 1969.
18. Burke, J. F., Dunn, J. L., & Scudder, K. R. (1969). *Pick-off for fluid angular rate sensor*. US3454023 A. July 08, 1969.
19. Neradka, V. F. (1970). *Ac vortex rate sensor*. US3529613 A. September 22, 1970.
20. Heilmann, T. G., Kwok, C. C. K., & Lapinas, Z. J. (1971). *Angular rate sensor*. US3604273 A. September 14, 1971.
21. Frederick, G. L. (1990). *Constant gain laminar jet angular rate sensing device*. US4945764 A. August 07, 1990.
22. Andreou, C., Pahitas, Y., & Georgiou, J. (2014). Bio-inspired micro-fluidic angular-rate sensor for vestibular prostheses. *Sensors, 14*(7), 13173–13185.
23. Andreou, C. M., Pahitas, Y., Pilavaki, E., & Georgiou, J. (2013). Bio-mimetic gyroscopic sensor for vestibular prostheses. In *2013 IEEE biomedical circuits and systems conference (BioCAS)*, pp. 17–20.
24. Liu, S., & Zhu, R. (2017). Micromachined fluid inertial sensors. *Sensors, 17*(2), 367.
25. Bosch, M. T., & Kishel, J. F. (1960). *Accelerometer*. 2,943,493. July 05, 1960.
26. Lees, S. (1961). *Null type integrating accelerometer*. US2988920 A. June 20, 1961.
27. Orrange, R. J. (1961). *Integrating accelerometer with digital readout*. 2,993,382. July 25, 1961.
28. Parker, B. (1962). *Gas bearing accelerometer*. 3,068,704. December 18, 1962.
29. Aske, V. H. (1964). *Accelerometer*. 3,142,990. August 04, 1964.
30. Entin, L. P. (1965). *Accelerometer*. 3,175,404. March 30, 1965.
31. Bentley, E. P., & Speas, C. A. (1965). *Acceleration sensitive device*. 3,195,357. July 20, 1965.
32. Raymond, H. A. (1970). *Fluid accelerometer*. 3,550,457. December 29, 1970.
33. Schmidlin, A. E. (1971). *Flueric accelerometer*. 3,577,786. May 04, 1971.
34. Leung, A. M., Jones, J., Czyzewska, E., Chen, J., & Pascal, M. (1997). Micromachined accelerometer with no proof mass. In *Technical digest, international electron devices meeting, 1997. IEDM'97*, pp. 899–902.
35. Leung, A. M., Jones, J., Czyzewska, E., Chen, J., & Woods, B. (1998). Micromachined accelerometer based on convection heat transfer. In *Proceedings of the eleventh annual international workshop on micro electro mechanical systems, 1998. MEMS 98*, pp. 627–630.
36. Tsang, S.-H., Ma, A. H., Karim, K. S., Parameswaran, A., & Leung, A. M. (2008). Monolithically fabricated polymermems 3-axis thermal accelerometers designed for automated wirebonder assembly. In *IEEE 21st international conference on micro electro mechanical systems, 2008. MEMS 2008*, pp. 880–883.
37. Povh, B., Rith, K., Scholz, C., Zetsche, F., & Rodejohann, W. (2015). *Particles and nuclei: An introduction to the physical concepts* (7th ed.). Berlin: Springer.
38. Duer, M. J. (2007). The basics of solid-state NMR. In M. J. Duer (Ed.), *Solid-state NMR spectroscopy principles and applications* (pp. 1–72). Hoboken, NJ: Wiley.
39. Larsen, M., & Bulatowicz, M. (2012). Nuclear magnetic resonance gyroscope: For DARPA's micro-technology for positioning, navigation and timing program. In *2012 IEEE international frequency control symposium proceedings*, pp. 1–5.
40. Kitching, J., Knappe, S., & Donley, E. A. (2011). Atomic sensors—A review. *IEEE Sensors Journal, 11*(9), 1749–1758.
41. Gauguet, A., Canuel, B., Lévèque, T., Chaibi, W., & Landragin, A. (2009). Characterization and limits of a cold atom Sagnac interferometer. *Physical Review A, 80*(6), 063604.
42. Lu, S., Chen, S., & Zhao, Y. (2010). MOEMS gyroscope based on acoustooptic mode coupling. In *Optical sensors and biophotonics II (2010), paper 79900I*, p. 79900I.
43. Trigona, C., Andò, B., & Baglio, S. (2016). Fabrication and characterization of an MOEMS gyroscope based on photonic bandgap materials. *IEEE Transactions on Instrumentation and Measurement, 65*(12), 2840–2852.
44. Zhang, B., & Li, W. F. (2012). Development of a micro accelerometer based MOEMS. In *2012 international conference on manipulation, manufacturing and measurement on the nanoscale (3 M-NANO)*, pp. 250–253.
45. Youssef, A., & El-Sheimy, N. *Gyroscope using torus shaped channels and image processing*. U.S. Patent Application 62/796,231. January 2019.
46. Youssef, A., & El-Sheimy, N. *Particle based accelerometer*. U.S. Patent Application 62/796,266. January 2019.
47. Delhaye, F. (2018). HRG by SAFRAN: The game-changing technology. In *2018 IEEE international symposium on inertial sensors and systems (INERTIAL)*, pp. 1–4.
48. Remillieux, G., & Delhaye, F. (2014). Sagem coriolis vibrating gyros: A vision realized. In *2014 DGON inertial sensors and systems (ISS)*, pp. 1–13.
49. Loper, E. J., Lynch, D. D., & Stevenson, K. M. (1986). *Projected performance of smaller hemispherical resonator gyros*. Presented at the PLANS'86—position location and navigation symposium, pp. 61–64.
50. Bodunov, B. P., Lopatin, V. M., Bodunov, S. B., & Kovshov, G. N. (1999). Gyroinclinometer for surveying during the drilling process. In *DGON proceedings, gyro technology symposium*, Stuttgart.
51. Jeanroy, A., & Leger, P. (2002). *Gyroscopic sensor and rotation measurement apparatus constituting an application thereof*. US6474161B1, November 05, 2002.
52. (2009). IEEE standard for inertial systems terminology. *IEEE Std 1559-2009*, pp. c1–c30.
53. Nassar, S. (2003). *Improving the inertial navigation system (INS) error model for INS and INS/DGPS applications*. PhD. Thesis, University of Calgary, Department of Geomatics Engineering, Calgary, Alberta, Canada.
54. Radi, A., Bakalli, G., Guerrier, S., El-Sheimy, N., Sesay, A. B., & Molinari, R. (2019). A multisignal wavelet variance-based framework for inertial sensor stochastic error modeling. *IEEE Transactions on Instrumentation and Measurement, 68*(12), 4924–4936.
55. Allan, D. W. (1966). Statistics of atomic frequency standards. *Proceedings of the IEEE, 54*(2), 221–230.
56. El-Sheimy, N., Hou, H., & Niu, X. (2008). Analysis and modeling of inertial sensors using Allan variance. *IEEE Transactions on Instrumentation and Measurement, 57*(1), 140–149.
57. Hou, H. (2004). *Modeling inertial sensors errors using allan variance*. M.Sc. Thesis, University of Calgary, Department of Geomatics Engineering, Calgary, Alberta, Canada.
58. Guerrier, S., Skaloud, J., Stebler, Y., & Victoria-Feser, M.-P. (2013). Wavelet-variance-based estimation for composite stochastic processes. *Journal of the American Statistical Association, 108*(503), 1021–1030.
59. Hansen, L. P. (1982). Large sample properties of generalized method of moments estimators. *Econometrica, 50*(4), 1029–1054.

Publisher's Note